

# Lateral Josephson effect on the surface of $\text{Co}_3\text{Sn}_2\text{S}_2$ magnetic Weyl semimetal

O.O. Shvetsov, V.D. Esin, Yu.S. Barash, A.V. Timonina, N.N. Kolesnikov, and E.V. Deviatov  
*Institute of Solid State Physics of the Russian Academy of Sciences,  
Chernogolovka, Moscow District, 2 Academician Ossipyan str., 142432 Russia*  
(Dated: September 20, 2019)

We experimentally study electron transport between two  $5\ \mu\text{m}$  spaced superconducting indium leads on a top of magnetic Weyl semimetal  $\text{Co}_3\text{Sn}_2\text{S}_2$ . For the disordered magnetic state of  $\text{Co}_3\text{Sn}_2\text{S}_2$  crystal, we only observe in the proximity of each of the leads the Andreev reflection, which is indicative of highly transparent In- $\text{Co}_3\text{Sn}_2\text{S}_2$  interfaces. If the sample is homogeneously magnetized, it demonstrates well-developed anomalous Hall effect state. In this regime, we detect the Josephson current even for  $5\ \mu\text{m}$  long junctions with unusual dependence of the critical current on the magnetic field and temperature. Since the anomalous Hall effect is related to the developed surface states in magnetic Weyl samples, we conclude that the topologically protected Fermi-arc states on the surface of  $\text{Co}_3\text{Sn}_2\text{S}_2$  substantially contribute to the proximity-induced spin-triplet Josephson current.

PACS numbers: 73.40.Qv 71.30.+h

## I. INTRODUCTION

Similarly to topological insulators<sup>1</sup> and quantum Hall systems<sup>2,3</sup>, Weyl semimetals<sup>4,5</sup> (WSM) have topologically protected surface states. They are Fermi arcs connecting projections of Weyl nodes on the surface Brillouin zone and these surface states inherit the chiral property of the Chern insulator edge states<sup>5</sup>. WSMs should have either space-inversion or time-inversion symmetry to be broken. First experimentally investigated WSMs were non-centrosymmetric crystals, where spin- and angle-resolved photoemission spectroscopy data have demonstrated spin-polarized surface Fermi arcs<sup>6,7</sup>.

There are only a few candidates of magnetically ordered materials<sup>4,8-10</sup> for the realization of WSMs in the systems with broken time reversal symmetry. Recently, giant anomalous Hall effect (AHE) was reported<sup>11,12</sup> for the kagome-lattice ferromagnet  $\text{Co}_3\text{Sn}_2\text{S}_2$  as an anomalous Hall conductance in zero magnetic field. The AHE can be regarded as the indication to a magnetic Weyl phase<sup>5</sup>, as supported by the topological-insulator-multilayer model, where the two-dimensional Chern edge states form the three-dimensional WSM surface states<sup>13</sup>. The Fermi arc surface states, indeed, were directly visualized in  $\text{Co}_3\text{Sn}_2\text{S}_2$  by scanning tunneling spectroscopy<sup>14</sup>.

For normal metals, Andreev reflection<sup>15</sup> allows charge transport from the metal (N) to superconductor (S) through the NS interface by creating a Cooper pair at energies below the superconducting gap<sup>15,16</sup>. For two closely spaced superconducting leads, i.e. for the SNS junction, multiple Andreev reflection can contribute to the subharmonic structure of the current-voltage characteristics<sup>16,17</sup>.

For topological materials, the proximity to a superconductor usually demonstrates non-trivial physics<sup>18-20</sup>. As it was experimentally shown, the Josephson coupling in a topological insulator is established through the surface conducting channels<sup>21</sup>. The edge current contribution can be retrieved even for systems with conducting bulk by analyzing the Josephson current behavior<sup>22-24</sup>. In

the Weyl semimetals, various topological superconducting states can appear<sup>25-28</sup> and various types of Andreev reflection can take place<sup>28,29</sup>, depending on the particular conditions. Thus the specular Andreev reflection, reminiscent the one in the graphene<sup>30,31</sup>, can take place at the Weyl semimetal - Weyl superconductor interface<sup>29</sup>, while the chirality blockade of Andreev reflection can appear at the interface of the magnetic Weyl semimetal and the conventional s-wave spin-singlet superconductor<sup>28</sup>.

For magnetically ordered topological materials the proximity to a superconductor is a new and emerging field involving the mutual influence of superconductivity and magnetism under nontrivial topological conditions, e.g., in the presence of topologically protected interface states. For example, it has been theoretically identified that the proximity to a superconductor can result in the Majorana modes originating from the Fermi arc in a Weyl semimetal wire with an axial magnetization<sup>32</sup>. It has also been predicted<sup>33</sup>, that the proximity induced superconducting surface states of magnetically doped topological insulators can represent chiral Majorana modes. Thus, it is reasonable to study proximity effects in superconducting junctions, fabricated on a three-dimensional magnetic Weyl semimetal surface.

Here, we experimentally study lateral electron transport between two  $5\ \mu\text{m}$  spaced superconducting indium leads on a top of magnetic Weyl semimetal  $\text{Co}_3\text{Sn}_2\text{S}_2$ . For the disordered magnetic state of  $\text{Co}_3\text{Sn}_2\text{S}_2$  crystal, we only observe the Andreev reflection in the proximity of each of the leads, which is indicative of highly transparent In- $\text{Co}_3\text{Sn}_2\text{S}_2$  interfaces. If the sample is homogeneously magnetized, it demonstrates well-developed anomalous Hall effect state. In this regime we find the Josephson current that takes place even for  $5\ \mu\text{m}$  long junctions and shows the unusual magnetic field and temperature dependencies. Since the anomalous Hall effect is related with developed Fermi-arc states in magnetic Weyl samples, we conclude that topologically protected paired states on the surface of  $\text{Co}_3\text{Sn}_2\text{S}_2$  substantially contribute to the Josephson current, which may require

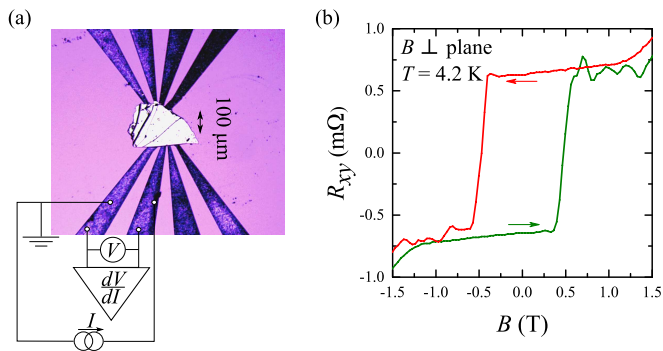


FIG. 1. (Color online) (a) A top-view image of the sample with the sketch of electrical connections. A flat (about  $100 \mu\text{m}$  size and  $1 \mu\text{m}$  thick) single-crystal  $\text{Co}_3\text{Sn}_2\text{S}_2$  flake is weakly pressed on the insulating  $\text{SiO}_2$  substrate with  $100 \text{ nm}$  thick,  $5 \mu\text{m}$  separated In leads. Non-linear  $dV/dI(I)$  curves are measured by a standard four-point technique, all the wire resistances are excluded. (b) Giant anomalous Hall effect, which confirms high quality of our  $\text{Co}_3\text{Sn}_2\text{S}_2$  samples<sup>11,12</sup>. Arrows indicate the field scanning directions.

the singlet-triplet conversion at the interfaces.

## II. SAMPLES AND TECHNIQUE

$\text{Co}_3\text{Sn}_2\text{S}_2$  single crystals were grown by the gradient freezing method. Initial load of high-purity elements taken in stoichiometric ratio was slowly heated up to  $920^\circ \text{C}$  in the horizontally positioned evacuated silica ampule, held for 20 h and then cooled with the furnace to the ambient temperature at the rate of  $20 \text{ deg/h}$ . The obtained ingot was cleaved in the middle part. The Laue patterns confirm the hexagonal structure with (0001) as cleavage plane. Electron probe microanalysis of cleaved surfaces and X-ray diffractometry of powdered samples confirmed stoichiometric composition of the crystal.

Despite it is possible to form contacts directly on the cleaved  $\text{Co}_3\text{Sn}_2\text{S}_2$  crystal plane, we use another technique, which is known to provide highly transparent contacts<sup>20,24,34</sup>. The leads pattern is formed on the insulating  $\text{SiO}_2$  substrate by lift-off technique after thermal evaporation of  $100 \text{ nm}$  In, see Fig. 1 (a). The indium leads are separated by  $5 \mu\text{m}$  intervals. Since the kagome-lattice ferromagnet  $\text{Co}_3\text{Sn}_2\text{S}_2$  can be easily cleaved along (0001) crystal plane, small (about  $100 \mu\text{m}$  size and  $1 \mu\text{m}$  thick)  $\text{Co}_3\text{Sn}_2\text{S}_2$  flakes are obtained by a mechanical cleaving method. Then we select the most plane-parallel flakes with clean surface, where no surface defects could be resolved with optical microscope. They are transferred to the In leads pattern and pressed slightly with another oxidized silicon substrate. A special metallic frame allows us to keep the substrates parallel and apply a weak pressure to the sample. No external pressure is needed for a  $\text{Co}_3\text{Sn}_2\text{S}_2$  flake to hold on to a substrate with In leads afterward. This procedure provides transparent contacts, stable in different cooling cycles, which

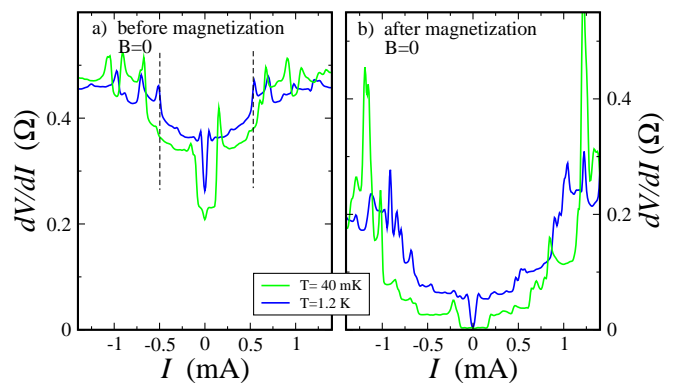


FIG. 2. (Color online) Examples of  $dV/dI(I)$  curves before sample magnetization (a) and after it (b), for the same sample in a single cooling cycle. Diminishing the temperature from  $1.2 \text{ K}$  to  $40 \text{ mK}$  has low effect on the initial Andreev-like  $dV/dI(I)$  curves in (a). Dashed lines indicate the wide  $dV/dI$  resistance drop, caused by Andreev reflection. In contrast, the magnetization procedure transforms  $dV/dI(I)$  curves into the Josephson-like ones in (b). The width of a wide zero-resistance region depends on the temperature below  $1.2 \text{ K}$ . The data are obtained in zero magnetic field.

has been also demonstrated before<sup>20,24,34</sup>.

Magnetoresistance measurements confirms high quality of the prepared  $\text{Co}_3\text{Sn}_2\text{S}_2$  samples. We check that samples demonstrate giant anomalous Hall effect, as it has been previously reported<sup>11,12</sup> for  $\text{Co}_3\text{Sn}_2\text{S}_2$  semimetal. Fig. 1 (b) shows hysteresis behavior and sharp switchings in Hall resistance  $R_{xy}$ , the switchings' positions  $\approx 0.5 \text{ T}$  even quantitatively coincide with the reported values<sup>11,12</sup>.

We study electron transport between two  $5 \mu\text{m}$  separated In leads by a standard four-point technique. The principal circuit diagram is depicted in Fig. 1 (a). In this connection scheme, all the wire resistances are excluded, which is necessary for low-impedance In- $\text{Co}_3\text{Sn}_2\text{S}_2$ -In junctions. To obtain  $dV/dI(I)$  characteristics, the dc current  $I$  (up to  $1 \text{ mA}$ ) is additionally modulated by a low ( $\approx 5 \mu\text{A}$ ) ac component. We measure both dc ( $V$ ) and ac ( $\sim dV/dI$ ) components of the voltage drop with a dc voltmeter and a lock-in, respectively, after a broadband preamplifier. The measurements are performed in a dilution refrigerator for the temperature interval  $30 \text{ mK}$ – $1.2 \text{ K}$ .

## III. EXPERIMENTAL RESULTS

$\text{Co}_3\text{Sn}_2\text{S}_2$  magnetic properties arise from the kagome-lattice cobalt planes, whose magnetic moments order ferromagnetically<sup>11</sup> out of plane below  $175 \text{ K}$ . Since the samples are cooled down from room temperature in zero magnetic field, the initial state of a macroscopic  $\text{Co}_3\text{Sn}_2\text{S}_2$  flake is magnetically disordered one, e.g., due to magnetic domains. The size of these domains is typically around the order of a micrometer<sup>35</sup> in  $\text{Co}_3\text{Sn}_2\text{S}_2$ ,

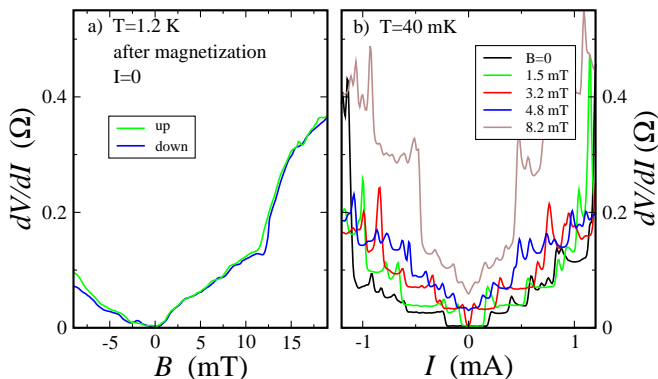


FIG. 3. (Color online) Suppression of the zero-resistance state by magnetic field. (a) Differential resistance  $dV/dI$  at zero dc current as a function of magnetic field. A finite zero-resistance region can be seen even at highest, 1.2 K, temperature. Two curves correspond to the opposite field sweep directions, they do not strictly coincide in the normal state. (b) Examples of  $dV/dI(I)$  characteristics for different magnetic fields at 40 mK. The zero-resistance region survives above 3.2 mT at this temperature. The magnetic field is perpendicular to the flake's plane. The sample is the same as in Fig. 2 (after magnetization).

which is much smaller than the distance between the indium leads in our samples. To obtain a definite AHE state of magnetically ordered WSM, the magnetization procedure is performed: an external magnetic field is swept slowly from -1.5 T to +1.5 T, both limits are far above the switching positions in Fig. 1 (b). Afterward, the external field goes down to zero.

Examples of  $dV/dI(I)$  characteristics are shown in Fig. 2 (a) and (b) before and after the magnetization procedure, respectively, for the same sample in a single cooling cycle.

Before magnetization, the curves demonstrate well known Andreev behavior. Since Andreev reflection allows subgap transport of Cooper pairs, it appears experimentally as the resistance drop for voltages within the superconducting gap<sup>16</sup>. As it can be seen in Fig. 2 (a), differential resistance is diminished within  $\approx \pm 5$  mA bias interval in respect to the normal resistance value  $\approx 0.5\Omega$ . The superconducting gap can be estimated from the width of this region as  $0.5 \text{ mA} \times 0.5 \Omega \approx 0.25 \text{ meV}$ . Since the bulk indium is known<sup>36</sup> to have the 0.5 meV gap, the obtained value is quite reasonable for the indium film on a top of ferromagnet. Temperature has low effect on  $dV/dI(I)$  curves, even at 40 mK the minimal resistance is not below one half of the normal value, see Fig. 2 (a).

The magnetization procedure changes the  $dV/dI(I)$  curves dramatically, see Fig. 2 (b): the zero-bias resistance value drops to zero. At low temperature of 40 mK, we observe a definite zero-resistance state in a wide current region, which qualitatively resembles the Josephson effect<sup>16</sup>. This behavior has been checked to be independent of the value and sign of the magnetization field.

As it is expected for the Josephson effect, the zero-resistance state can also be suppressed by magnetic field. Even at the highest temperature, the junction resistance is zero in a finite,  $\pm 1$  mT field interval, see Fig. 3 (a). This behavior is demonstrated in detail in Fig. 3 (b) for  $dV/dI(I)$  curves at lowest temperature of 40 mK. The zero-resistance state survives up to 3.2 mT, which is much below the critical indium field<sup>37</sup> of about 40 mT. Above 3.2 mT field,  $dV/dI(I)$  curves demonstrate usual Andreev behavior, so the indium leads are still superconducting.

Thus, we demonstrate in Figs. 2 and 3, that two superconducting contacts induce Josephson current in an unprecedentedly long  $L = 5 \mu\text{m}$  In-Co<sub>3</sub>Sn<sub>2</sub>S<sub>2</sub>-In junction. The above described behavior can be reproduced for different samples, see, e.g., Fig. 4. In this case, the normal  $dV/dI$  resistance is one order higher, about 3 Ohm, as depicted in the main field in Fig. 4 (a). The differential resistance is diminished within  $\pm 0.075$  mA interval, which gives the same  $0.075 \text{ mA} \times 3 \Omega \approx 0.25 \text{ meV}$  superconducting gap value. Before sample magnetization,  $dV/dI$  is always finite even at 40 mK, see Fig. 4 (a), while it drops to zero after the magnetization procedure.

We also observe unusual behavior of the temperature and magnetic field dependencies of the critical current  $I_c$ . To obtain  $I_c$  values with high accuracy for given  $(B, T)$  values, we sweep current  $I$  ten times from zero (superconducting state) to above  $I_c$  (resistive state), and then determine  $I_c$  as an average value of  $dV/dI$  jump positions in different sweeps. Lower currents are more suitable for accurate determination of  $I_c$ , so the results are presented in the insets to Fig. 4 (a) and (b). All the experimental points are well reproducible, variation of  $I_c$  in different sweeps is below the symbol size in the inset.

$I_c(T)$  demonstrates weak temperature dependence below 0.75 K, while  $I_c$  is diminishing strongly above it to one half of the initial value at our highest 1.2 K, see the inset to Fig. 4 (a). This dependence can be crudely extrapolated to  $\approx 2$  K critical temperature, which well correspond to the 0.25 meV superconducting gap, determined from the Andreev curve in Fig. 4 (a). However,  $I_c(T)$  is very unusual, it does not demonstrate the conventional for long diffusive SNS junctions exponential decay<sup>38,39</sup>. The experimental  $I_c(T)$  is more close to the results for Josephson junctions with spin-flip scattering<sup>40</sup>.

The zero-resistance state at  $I = 0$  is suppressed by magnetic field at  $\pm 7$  mT, see Fig. 4 (b). The full  $I_c(B)$  pattern is depicted in the inset to Fig. 4 (b). At lowest temperatures,  $I_c(B)$  is changing very slowly (within 10%) until  $\pm 7$  mT, but falls to zero above this value. The characteristic feature is that the low-field  $I_c(B)$  dependence is antisymmetric in respect to the zero field. This behavior is confirmed by extremely slow field sweep with a large amount of points, as demonstrated by open circles in the inset. There are also some  $I_c(B)$  oscillations within the  $\pm 7$  mT interval. Both the antisymmetry and the oscillations are destroyed by temperature above 0.75 K. The shallow oscillations in  $I_c(B)$  could be related with usual

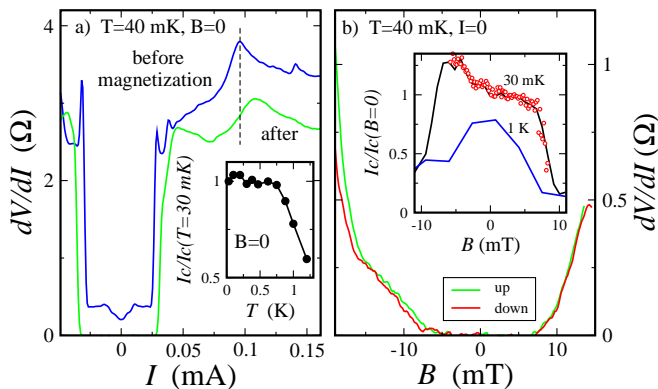


FIG. 4. (Color online) Experimental results for a different sample at minimal 40 mK temperature. (a) Formation of the Josephson-type curve (the green one) with well-defined critical current after sample magnetization. Dashed line indicates the superconductive gap position. Inset demonstrates temperature dependence of the critical current, which is unusual for long diffusive Josephson junctions. (b) Suppression of the zero-resistance state by magnetic field at zero dc current for two opposite field sweep directions. Inset demonstrates critical current as a function of magnetic field for two different temperatures. At 40 mK, the  $I_c(B)$  is not symmetric at low fields, but symmetrically falls to zero at  $\pm 7$  mT. The asymmetry is confirmed by extremely slow field sweep with a low step, as demonstrated by open circles. The expected  $I_c(B)$  symmetry is restored above 1 K. The magnetic field is perpendicular to the flake's plane.

interference effects<sup>16</sup>, although the corresponding curve substantially differs from the standard pattern<sup>41</sup> and no strong suppression of  $I_c(B)$  at  $B < \pm 7$  mT is observed.

It is important, that both for the resistance at  $I = 0$  in the main Fig. 4 (b) and for significant current  $\approx 0.05$  mA in the inset, the Josephson effect is destroyed under the same magnetic fields  $\pm 7$  mT. Thus, there is no sample overheat in  $I_c(B, T)$  measurements, so the unusual  $I_c(T)$  temperature dependence is correct in the inset to Fig. 4 (a).

#### IV. DISCUSSION

As a result, we demonstrate the Josephson current through the magnetically ordered  $5\mu\text{m}$  long In- $\text{Co}_3\text{Sn}_2\text{S}_2$ -In junctions, where  $\text{Co}_3\text{Sn}_2\text{S}_2$  flake is in a definite AHE state. On the other hand, no supercurrent can be observed in these junctions, when  $\text{Co}_3\text{Sn}_2\text{S}_2$  is in the disordered magnetic state. This effect is well reproducible for different samples, see Figs. 2 and 4 (a).

First of all, we should exclude possible fabrication defects, like parasite indium connections in the junction plane:

(i) The thickness of the indium film is chosen to be much smaller than the leads separation ( $100\text{ nm} \ll 5\mu\text{m}$ ) to avoid shorting of In leads in lift-off.

(ii) The crucial argument against the presence of any

leakage is a pronounced dependence of the Josephson effect on the WSM magnetization. For conventional superconductors like indium, the proximity to a ferromagnet weakens superconductivity. Just opposite to the known indium behavior, magnetically ordered state of  $\text{Co}_3\text{Sn}_2\text{S}_2$  enhances the Josephson coupling.

Thus, one can be sure that the observed Josephson current flows through the proximity-influenced magnetically ordered  $\text{Co}_3\text{Sn}_2\text{S}_2$  WSM.

The surface states transport can be a key point to explain our experimental results. In the case of  $\text{Co}_3\text{Sn}_2\text{S}_2$ , Fermi-arc surface states have been directly identified by scanning tunneling spectroscopy<sup>14</sup>. The giant anomalous Hall effect is interpreted in terms of the surface states<sup>5</sup>, and we observe the Josephson effect just after magnetization procedure, i.e. for a well pronounced AHE state, see Fig. 1 (b). Therefore, Weyl surface states exist along the macroscopic  $\text{Co}_3\text{Sn}_2\text{S}_2$  flake. Their proximity-induced pairing results in the effective supercurrent-carrying channels. The important role of the chiral surface channels in the Josephson transport studied is also supported by their topological protection and the lateral geometry of the junction.

The magnetic domain structure in  $\text{Co}_3\text{Sn}_2\text{S}_2$  flake can have a substantial influence on the junction's properties. When the domain magnetization in the  $\text{Co}_3\text{Sn}_2\text{S}_2$  sample is disordered just after the sample cooling, the chirality of Weyl nodes can switch across the magnetic domain walls<sup>5</sup> and a continuous surface state can only appear along a single magnetic domain, which size is around the order of a micrometer<sup>35</sup>. Such a disordered magnetic structure should produce significant disordered spin-flip processes and can prevent the Josephson effect to develop between the  $5\mu\text{m}$  spaced indium leads, allowing only the observation of Andreev reflection in the proximity of each of the leads, in accordance with our measurements for samples before the magnetization procedure.

While in topological insulators the surface conducting channels have been experimentally identified as dominating in establishing the Josephson coupling<sup>21</sup>, the Josephson current in Weyl semimetals can be transferred generally via both the surface and the bulk channels. The two contributions could have different characteristics and jointly result in unusual critical current dependence on the magnetic field and the temperature. Although the latter point, as well as the identification of the particular type of proximity-induced pairing within the magnetic Weyl semimetal  $\text{Co}_3\text{Sn}_2\text{S}_2$  flake, requires further theoretical and experimental investigations, some other important features of the problem can be made clear.

Since the Weyl surface states are spin-polarized<sup>5,14,42</sup> and  $\text{Co}_3\text{Sn}_2\text{S}_2$  itself is a strong ferromagnet or even a half-metal<sup>42</sup>, one can expect a triplet supercurrent<sup>43-45</sup> through  $\text{Co}_3\text{Sn}_2\text{S}_2$  surface and bulk channels. When singlet Cooper pairs from the superconductor are converted into triplet pairs within the spin-polarized material, a long-range proximity effect, as known, can take place: while the singlet component penetrates into the

ferromagnet over a short length<sup>46</sup>  $\xi_h = (D/h)^{1/2}$  ( $h$  is the exchange field and  $D$  the diffusion coefficient), the triplet component penetrates over a much longer length  $(D/\epsilon)^{1/2}$ , which is of the same order as that for the penetration of the superconducting pairs into a normal metal<sup>43</sup>. This conclusion prohibits, in particular, the conventional long-range s-wave spin-singlet pairing in  $\text{Co}_3\text{Sn}_2\text{S}_2$  flake, which occurs in In and cannot be present in the magnetic Weyl semimetal, as also follows from the chirality blockade arguments<sup>28</sup>. Since the exchange field and spin-orbit coupling are jointly present in Weyl semimetals, the singlet-triplet conversion at its interface does not require additional magnetic inhomogeneities<sup>47,48</sup>. These predictions are consistent with our observation of the Josephson current in  $5 \mu\text{m}$  long In- $\text{Co}_3\text{Sn}_2\text{S}_2$ -In junctions.

The triplet supercurrent can be responsible for the low-field  $I_c(B)$  antisymmetry in the inset to Fig. 4 (b). The low-field variation of  $I_c(B)$  reflects the magnetization dynamics in the bulk  $\text{Co}_3\text{Sn}_2\text{S}_2$ , since in the inset to Fig. 4 (b)  $I_c$  is smaller for positive fields and for positively magnetized flake. As opposed to the low-field region, the fields exceeding  $B_c \approx \pm 7 \text{ mT}$  can be considered as destroying the superconducting pairing via the surface channels, where the topologically protected magnetic ordering is not sensitive to the lower values of the external field.

## V. CONCLUSION

As a conclusion, we experimentally study electron transport between two  $5 \mu\text{m}$  spaced superconducting indium leads on a top of magnetic Weyl semimetal  $\text{Co}_3\text{Sn}_2\text{S}_2$ . For the disordered magnetic state of  $\text{Co}_3\text{Sn}_2\text{S}_2$  crystal, we only observe in the proximity of each of the leads the Andreev reflection, which is indicative of highly transparent In- $\text{Co}_3\text{Sn}_2\text{S}_2$  interfaces. If the sample is homogeneously magnetized, it demonstrates well-developed anomalous Hall effect state. In this regime, we detect the Josephson current even for  $5 \mu\text{m}$  long junctions with unusual dependence of the critical current on the magnetic field and temperature. Since the anomalous Hall effect originates from the developed surface states in magnetic Weyl samples, we conclude that the topologically protected spin-polarized Fermi-arc states on the surface of  $\text{Co}_3\text{Sn}_2\text{S}_2$  substantially contribute to the proximity-induced spin-triplet lateral Josephson current.

## ACKNOWLEDGMENTS

We wish to thank V.T. Dolgoplov for fruitful discussions, and S.V. Simonov for X-ray sample characterization. We gratefully acknowledge financial support partially by the RFBR (project No. 19-02-00203), RAS, and RF State task.

- 
- <sup>1</sup> M. Z. Hasan and C. L. Kane, Rev. Mod. Phys. 82, 3045 (2010).
- <sup>2</sup> M. Büttiker, Phys. Rev. B **38**, 9375 (1988).
- <sup>3</sup> E. V. Deviatov, Physics-Uspekhi 50 (2) 197 (2007).
- <sup>4</sup> X. Wan, A. M. Turner, A. Vishwanath, S. Y. Savrasov, Phys. Rev. B 83, 205101 (2011).
- <sup>5</sup> For a review on topological semimetals, see N.P. Armitage, E.J. Mele, and A. Vishwanath, Rev. Mod. Phys. 90, 015001 (2018).
- <sup>6</sup> P.K. Das, D.D. Sante, I. Vobornik, J. Fujii, T. Okuda, E. Bruyer, A. Gyenis, B.E. Feldman, J. Tao, R. Ciancio, G. Rossi, M.N. Ali, S. Picozzi, A. Yazdani, G. Panaccione, and R.J. Cava, Nature Comm. 7, 10847 (2016).
- <sup>7</sup> B. Feng, Y.-H. Chan, Y. Feng, R.-Y. Liu, M.-Y. Chou, K. Kuroda, K. Yaji, A. Harasawa, P. Moras, A. Barinov, W. Malaeb, C. Bareille, T. Kondo, S. Shin, F. Komori, T.-C. Chiang, Y. Shi, and I. Matsuda, Phys Rev B 94, 195134 (2016).
- <sup>8</sup> M. Hirschberger, S. Kushwaha, Z. Wang, Q. Gibson, S. Liang, C. A. Belvin, B. A. Bernevig, R. J. Cava, N. P. Ong, Nat. Mater. 15, 1161-1165 (2016).
- <sup>9</sup> G. Xu, H. Weng, Z. Wang, X. Dai, Z. Fang, Phys. Rev. Lett. 107, 186806 (2011).
- <sup>10</sup> S. K. Kushwaha, Z. Wang, T. Kong, R. J. Cava, J. Phys. Condens. Matter. 30, 075701 (2018).
- <sup>11</sup> Enke Liu, Yan Sun, Nitesh Kumar, Lukas Muechler, Aili Sun, Lin Jiao, Shuo-Ying Yang, Defa Liu, Aiji Liang, Qian Xu, Johannes Kroder, Vicky Süß, Horst Borrmann, Chandra Shekhar, Zhaosheng Wang, Chuanying Xi, Wenhong Wang, Walter Schnelle, Steffen Wirth, Yulin Chen, Sebastian T. B. Goennenwein, and Claudia Felser, Nature Physics 14, 1125 (2018).
- <sup>12</sup> Qi Wang, Yuanfeng Xu, Rui Lou, Zhonghao Liu, Man Li, Yaobo Huang, Dawei Shen, Hongming Weng, Shancai Wang and Hechang Lei, Nature Communications 9, 3681 (2018).
- <sup>13</sup> A. A. Burkov, Leon Balents, Phys. Rev. Lett. 107, 127205 (2011).
- <sup>14</sup> Noam Morali, Rajib Batabyal, Pranab Kumar Nag, Enke Liu, Qiunan Xu, Yan Sun, Binghai Yan, Claudia Felser, Nurit Avraham, Haim Beidenkopf, arXiv:1903.00509
- <sup>15</sup> A. F. Andreev, Soviet Physics JETP **19**, 1228 (1964).
- <sup>16</sup> M. Tinkham, Introduction to Superconductivity (2d ed., McGrawHill, New York, 1996).
- <sup>17</sup> N. Agrait, A. Levy Yeyati, and J. M. van Ruitenbeek, Phys. Rep. 377, 81 (2003).
- <sup>18</sup> L. Fu and C. L. Kane, Phys. Rev. Lett. 100, 96407 (2008).
- <sup>19</sup> A. Kononov, V.A. Kostarev, B.R. Semyagin, V.V. Preobrazhenskii, M.A. Putyato, E.A. Emelyanov, and E.V. Deviatov, Physical Review B 96, 245304 (2017). DOI: 10.1103/PhysRevB.96.245304
- <sup>20</sup> A. Kononov, O.O. Shvetsov, S.V. Egorov, A.V. Timonina, N.N. Kolesnikov and E.V. Deviatov EPL, 122, 27004 (2018)

- <sup>21</sup> Jae Hyeong Lee, Gil-Ho Lee, Joonbum Park, Janghee Lee, Seung-Geol Nam, Yun-Sok Shin, Jun Sung Kim, and Hu-Jong Lee *Nano Letters*, 14(9), 50295034 (2014). <http://doi.org/10.1021/nl501481b>
- <sup>22</sup> Sean Hart, Hechen Ren, Timo Wagner, Philipp Leubner, Mathias Mhlbauer, Christoph Brne, Hartmut Buhmann, Laurens W. Molenkamp & Amir Yacoby, *Nature Physics* 10, 638643 (2014), doi:10.1038/nphys3036
- <sup>23</sup> Vlad S. Pribiag, Arjan J. A. Beukman, Fanming Qu, Maja C. Cassidy, Christophe Charpentier, Werner Wegscheider & Leo P. Kouwenhoven, *Nature Nanotechnology* 10, 593 (2015)
- <sup>24</sup> O.O. Shvetsov, A. Kononov, A.V. Timonina, N.N. Kolesnikov, E.V. Deviatov, *JETP Letters*, 107, 774779 (2018); *EPL*, 124, 47003 (2018).
- <sup>25</sup> T. Meng and L. Balents, *Phys. Rev. B* 86, 054504 (2012).
- <sup>26</sup> G. Y. Cho, J. H. Bardarson, Y.-M. Lu, and J. E. Moore, *Phys. Rev. B* 86, 214514 (2012).
- <sup>27</sup> H. Wei, S. P. Chao, and V. Aji, *Phys. Rev. B* 89, 014506 (2014).
- <sup>28</sup> N. Bovenzi, M. Breitzkreiz, P. Baireuther, T. E. O'Brien, J. Tworzydło, I. Adagideli, and C. W. J. Beenakker, *Phys. Rev. B* 96, 035437 (2017).
- <sup>29</sup> Wei Chen, Liang Jiang, R. Shen, L. Sheng, B. G. Wang, D. Y. Xing *EPL* 103, 27006 (2013).
- <sup>30</sup> C. W. J. Beenakker, *Physical Review Letters* 97, 067007 (2006).
- <sup>31</sup> C. W. J. Beenakker, *Reviews of Modern Physics* 80, 1337 (2008).
- <sup>32</sup> P Baireuther, J Tworzydło, M Breitzkreiz, I Adagideli and CW J Beenakker, *New J. Phys.* 19, 025006 (2017).
- <sup>33</sup> Tsubasa Toki, Sho Nakosai, Yukio Tanaka, Yuki Kawaguchi, arXiv:1906.01934
- <sup>34</sup> O. O. Shvetsov, V. D. Esin, A. V. Timonina, N. N. Kolesnikov, and E. V. Deviatov *Phys. Rev. B* 99, 125305 (2019)
- <sup>35</sup> Qiunan Xu, Enke Liu, Wujun Shi, Lukas Muechler, Jacob Gayles, Claudia Felser, and Yan Sun *PRB* 97, 235416 (2018)
- <sup>36</sup> A. M. Toxen *Phys. Rev.* 123, 442 (1961)
- <sup>37</sup> P. Scharnhorst *Phys. Rev. B* 1, 4295 (1970).
- <sup>38</sup> I. O. Kulik, *Sov. Phys. JETP* 30, 944 (1970).
- <sup>39</sup> P. Dubos, H. Courtois, B. Pannetier, F. K. Wilhelm, A. D. Zaikin, and G. Schön *Phys. Rev. B* 63, 064502 (2001).
- <sup>40</sup> J. C. Hammer, J. C. Cuevas, F. S. Bergeret, and W. Belzig, *Phys. Rev. B* 76, 064514 (2007).
- <sup>41</sup> A. Barone and G. Paterno, *Physics and Applications of the Josephson Effect* (John Wiley&Sons, New York, 1982).
- <sup>42</sup> Lin Jiao, Qiunan Xu, Yeryun Cheon, Yan Sun, Claudia Felser, Enke Liu, and Steffen Wirth *Phys. Rev. B* 99, 245158 (2019).
- <sup>43</sup> F. S. Bergeret, A. F. Volkov, and K. B. Efetov, *Phys. Rev. Lett.* 86, 4096 (2001).
- <sup>44</sup> F. S. Bergeret, A. F. Volkov, and K. B. Efetov, *Rev. Mod. Phys.* 77, 1321 (2005).
- <sup>45</sup> R. S. Keizer, S. T. B. Goennenwein, T. M. Klapwijk, G. Miao, G. Xiao and A. Gupta, *Nature* 439, 825 (2006).
- <sup>46</sup> A. I. Buzdin, *Rev. Mod. Phys.* 77, 935 (2005).
- <sup>47</sup> F. S. Bergeret and I. V. Tokatly, *Phys. Rev. Lett.* 110, 117003 (2013).
- <sup>48</sup> F. S. Bergeret and I. V. Tokatly, *Phys. Rev. B* 89, 134517 (2014).